Nickel and Scandium-Bearing Minerals Associated with Limonitic Laterite Zone of the Lameruru Deposit in Southeast Sulawesi, Indonesia

Jance Murdjani Supit[1,4], Arifudin Idrus[1*], Himawan Tri Bayu Murti Petrus[2], I Gde Sukadana[3], and Fadiah Pratiwi[3]

[1]Department of Geological Engineering, Faculty of Engineering, Universitas Gadjah Mada, Yogyakarta 55281, Indonesia
[2]Department of Chemical Engineering (Sustainable Mineral Processing Research Group), Faculty of Engineering, Universitas Gadjah Mada, Yogyakarta, 55281, Indonesia
[3]Research Center for Nuclear Materials and Radioactive Waste Technology, National Research and Innovation Agency (BRIN), Gd.720 KST BJ.Habibie, PUSPIPTEK, Serpong, Tangerang Selatan, Banten, Indonesia
[4]Department of Mining Engineering, Faculty of Mining and Petroleum Engineering, Universitas Papua, Manokwari, Papua Barat, 98314, Indonesia

Corresponding author: arifidrus@ugm.ac.id
Manuscript received: December, 9, 2024; revised: February, 11, 2025;
approved: May, 26, 2025; available online: June, 16, 2025

Abstract - This study investigates nickel and scandium enrichment within a laterite profile developed on ultramafic rocks in the Lameruru area, Southeast Sulawesi. Utilizing mineralogical and geochemical analyses, the research examines transformations from parent rock through four laterite horizons: rocky saprolite, earthy saprolite, yellow limonite, and red limonite. Results reveal distinct enrichment patterns for Ni and Sc. Nickel is concentrated in the saprolite, hosted by minerals such as willemseite, vermiculite, lizardite, and antigorite, and decreases towards the red limonite, suggesting an initial enrichment during weathering followed by remobilization. Conversely, Sc increases throughout the profile, peaking in the red limonite and dominantly associated with goethite. Nickel is structurally bound within mineral lattices, while scandium is adsorbed onto mineral surfaces, particularly goethite in the red limonite. This contrasting behaviour highlights different geochemical controls influencing Ni and Sc enrichment during lateritization. Further research should explore these mechanisms to optimize recovery strategies.

Keywords: Lameruru, limonite, nickel-scandium-bearing minerals, Southeast Sulawesi

INTRODUCTION

The Lameruru lateritic nickel deposit has developed through the extensive process of lateritization, which has transformed the underlying Cretaceous ultramafic rocks within the East Sulawesi ophiolite belt (Fu *et al*., 2014). This ophiolite belt is one of the four primary lithotec-tonic belts that make up the complex geological framework of the Sulawesi Island (Kadarusman *et al*., 2004; Maulana *et a*l., 2014; Mawaleda *et al.,* 2018). The lateritization process has significantly enriched the nickel content in the saprolite layer by up to thirty times, and the scandium content in the limonite layer by up to nine times, compared to the parent ultramafic rock (Butt and

Wang, 2013; Sanematsu *et al*., 2017; Maulana *et al*, 2019).

Limonite, the uppermost section of the lateritic nickel deposit, is characterized by its high iron content, and also contains substantial amounts of other valuable metals, such as chromium, cobalt, and the critical metals nickel and scandium (Hughes *et al*., 2020). Nickel and scandium are considered critical metals due to their high demand in modern advanced industries. Nickel is essential for the production of stainless steel, jet engines, and electric vehicle batteries (Sharma, 2021; Czerwiński, 2022; Dilshara *et al.,* 2023). While scandium has numerous applications in the aerospace industry, including the manufacture of durable and lightweight sporting equipment, electronics, and solid fuel cells (Røyset and Ryum, 2005; Emsley, 2014; Toropova *et al.,* 2017). The widespread utilization of Ni and Sc in these advanced industries highlights the importance of ongoing exploration efforts to identify new sources of these valuable resources, ensuring their continued availability and supply. Therefore, an advanced characterization of Ni-Sc-bearing minerals is crucial to be done, and such kind of studies are still limited including in the studied area.

This study is aimed to provide a comprehensive understanding of the Lameruru lateritic nickel deposit, encompassing its mineral association, and the specific Ni-Sc-bearing minerals present. To achieve this objective, detailed mineralogical, geochemical, and mineral chemical analyses on samples retrieved from Melati Pit at the Lameruru nickel laterite mining area were performed. The findings of this study will significantly enhance the understanding of Ni and Sc distributions within lateritic nickel deposits derived from ultramafic rocks, as well as provide valuable insights into the strategic planning and development of future mining operations in similar geological settings.

Regional Geology

The Lameruru area is located within the East Sulawesi ophiolite belt, which constitutes one of the four geological provinces of Sulawesi (Hall and Wilson, 2000). Lameruru is incorporated within the Lasusua-Kendari regional geological map sheet (Rusmana *et al*., 1993). The rock formations of the Lameruru region and its vicinity, arranged from the younger to the older one, are including alluvium, Pandua Formation, Salodik Formation, Matano Formation, Ophiolite Complex, and Tokala Formation (Rusmana *et al*., 1993).

The detailed characteristics of those formations are described in order from younger to older are as follows. Alluvium (Qa) comprises pebbles, gravel, sand, and clay, dating to the Holocene age. The Pandua Formation (Tmpp) consists of conglomerate, sandstone, and claystone, dating from the Late Miocene to the Pliocene age. The Salodik Formation (Tems) composed of calcilutite and oolitic limestone, is dated from Late Eocene to Oligocene age. The Matano Formation (Km) made up of calcilutite with shale and chert intercalation, is considered to be of Cretaceous age. Ophiolite rocks (Ku) comprise peridotite, dunite, and serpentinite. Estimated to date from the Triassic to Early Jurassic period (Rusmana *et al*., 1993) (Figure 1a), the Tokala Formation (TRJt) comprises calcilutite, limestone, sandstone, shale, marl, and slate.

The ultramafic rocks of the East Sulawesi ophiolite belt, composed of primarily serpentinized peridotite, have undergone extensive lateritization, resulting in the formation of the Lameruru lateritic nickel deposit (Kadarusman *et al*., 2004; Maulana *et al*., 2014). This study is focused on the Ni-Sc-bearing minerals associated with the lateritic zone as a chemical weathering product of the rock type.

Geological Characteristics of the Lameruru Deposit

The studied area at the Lameruru lateritic nickel mine is situated within the Melati Pit, covering an area of approximately 2.3 ha (Figure 1.b). The parent rock of the Lameruru lateritic nickel deposit predominantly consist of peridotite, a type of ultramafic rock characterized by its distinctive blackish-green colour. This peridotite
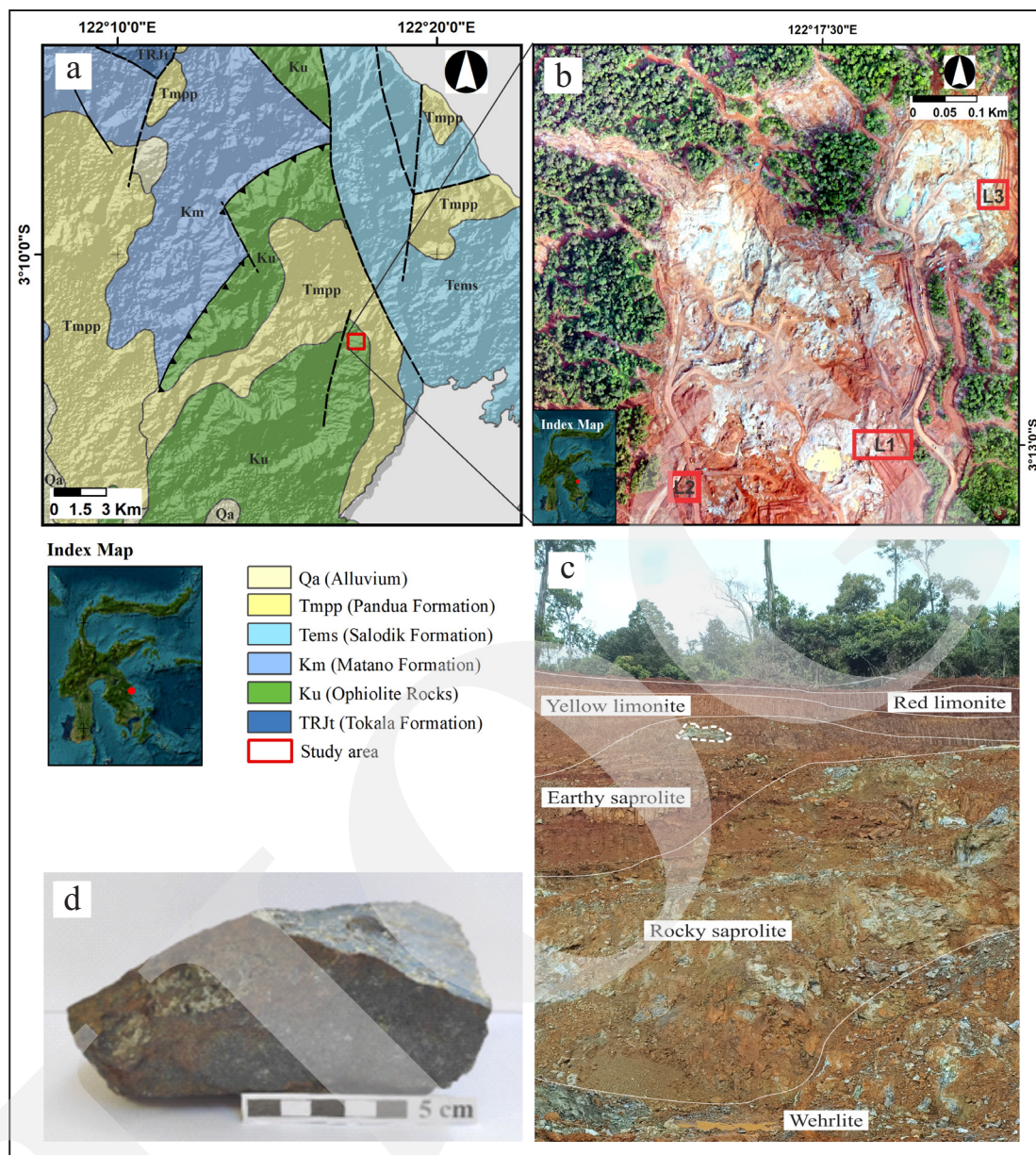
Figure 1. a) Regional geological map of Lameruru area (after Rusmana *et al.*, 1993), b) Sample location in Melati Pit at Lameruru mining area, c) Laterite profile of Melati Pit, d) Parent rock (wehrlite) from Melati Pit.

is holocrystalline, and is remarkably compact and solid in nature. The constituent minerals of the peridotite include olivine and pyroxene altered to epidote and chlorite, associated with various ore minerals, exhibit a diverse range of grain sizes from fine to coarse.

The extensive process of lateritization, which has transformed the underlying Cretaceous ultramafic rocks within East Sulawesi ophiolite belt, has produced the Lameruru lateritic nickel deposit, exceeding 20 m in the total thickness.

This lateritic profile can be categorized into five distinct zones: the parent rock, rocky saprolite, earthy saprolite, yellow limonite, and red limonite (Figure 1c), each with its own unique mineralogical and geochemical characteristics (Fu *et al.*, 2014). Microscopically, the parent rock in Melati Pit at the Lameruru lateritic nickel deposit is predominantly of wehrlite (Figure 1d), which has been extensively altered and transformed through the process of lateritization (Butt and Wang, 2013).

177

Material and Methods

Twenty samples were collected from different side and profile of Melati Pit at the Lameruru Ni laterite mining area (7 samples from L1; 4 samples from L2, and 9 samples from L3). Three samples for petrography analysis to determine the composition of rock-forming minerals. The samples were analyzed using an Olympus BX51 polarizing microscope.

Twenty samples were analyzed using micro-XRF from Bruker and AMICS software (Advanced Mineral Identification and Characterization System) to determine the mineral composition and distribution of laterite zones. The samples were analyzed under vacuum conditions, high voltage 50 kV, anode current 600 µA, and maximum pulse throughout 275,000 cps. The mapping area is 16x16 mm, with a 30 µm pixel size for 2.5 hours.

Petrography and micro-XRF analyses were conducted at the Laboratory of the Centre for Research on Nuclear Fuel Cycle and Radioactive Waste, National Research Institute (BRIN), Indonesia.

Twenty samples were analyzed by XRF to determine the major oxide composition and the level of ultramafic alteration in the studied area. Those twenty samples were analyzed by ICP-MS to determine the Ni-Sc content in the laterite zones. XRF and ICP-MS analyses were conducted at the Indo Mineral Research (IMR) Laboratory, Indonesia.

Rock forming, altered minerals, and Ni-Sc distribution of five samples were analyzed by electron probe micro-analyzer (EPMA) method using JEOL JXA-ISP100, in the Engineering Research Innovation Centre (ERIC) Laboratory, Universitas Gadjah Mada, Indonesia. EPMA analysis used polished thin section with the coating of carbon. The analysis used an accelerating voltage of 15 kV, probe current of 12 nA, 1 µm beam diameter, and element detection limit of 0,001 %. Standard natural mineral samples of MAC 15299 were used to analyze mineral chemistry based on major oxides, and MAC 16704 to analyze nickel and scandium content. Both of them were used as standards for the quantitative correction method. List of samples analyzed is shown by Table 1.

Table 1. List of Samples, their Methods, and Location According to Figure 1b

Sample code	Sample types	Analyses	Location
RL020120	Red limonite	micro-XRF, XRF, ICP-MS	L1
RL020119	Red limonite	micro-XRF, XRF, ICP-MS, EPMA	L1
RL020117	Red limonite	micro-XRF, XRF, ICP-MS	L1
ES020113	Earthy saprolite	micro-XRF, XRF, ICP-MS, EPMA	L1
ES020105	Earthy saprolite	micro-XRF, XRF, ICP-MS	L1
RS020101	Rocky saprolite	micro-XRF, XRF, ICP-MS, EPMA	L1
PR0201	Wehrlite	Petrography, micro-XRF, XRF, ICP-MS, EPMA	L1
RL020206	Red limonite	micro-XRF, ICP-MS	L2
RL020205	Red limonite	micro-XRF, XRF, ICP-MS	L2
RL020201	Red limonite	micro-XRF, XRF, ICP-MS	L2
PR0202	Wehrlite	Petrography, micro-XRF, XRF, ICP-MS	L2
RL020323	Red limonite	micro-XRF, XRF, ICP-MS	L3
RL020321	Red limonite	micro-XRF, XRF, ICP-MS	L3
YL020318	Yellow limonite	micro-XRF, XRF, ICP-MS, EPMA	L3
YL020312	Yellow limonite	micro-XRF, XRF, ICP-MS	L3
YL020309	Yellow limonite	micro-XRF, XRF, ICP-MS	L3
ES020308	Earthy saprolite	micro-XRF, XRF, ICP-MS	L3
ES020305	Earthy saprolite	micro-XRF, XRF, ICP-MS	L3
RS020301	Rocky saprolite	micro-XRF, XRF, ICP-MS	L3
PR0203	Wehrlite	Petrography, micro-XRF, XRF, ICP-MS	L3

RESULTS

Mineralogy of Parent Rock

The petrographic analysis reveals that the parent rock in the Melati Pit is wehrlite (L1−L2) and wehrlite altered to serpentinite (L3). Wehrlite is a type of peridotite composed primarily of the essential rock-forming minerals of clinopyroxene, orthopyroxene, and olivine (Figures 2a-b; c-d). These primary minerals make up the bulk of the peridotite mineralogical assemblage. In addition, the peridotite contains a suite of accessory minerals such as spinel, chromite, and alteration minerals such as serpentine and chlorite, which are present in smaller quantities, but contribute to the overall complexity of the rock composition. In contrast, wehrlite altered to serpentinite (Figures 2e-f) is dominated by alteration minerals such as antigorite and several primary minerals such as olivine, as well as additional minerals such as chromite. The detailed micro-XRF mineral mapping results further identify the presence of several minor mineral phases, such as aegirine-augite, ferritschermakite, hedenbergite, lizardite, and maghemite (Figure 3). The identification of these less abundant mineral constituents provides
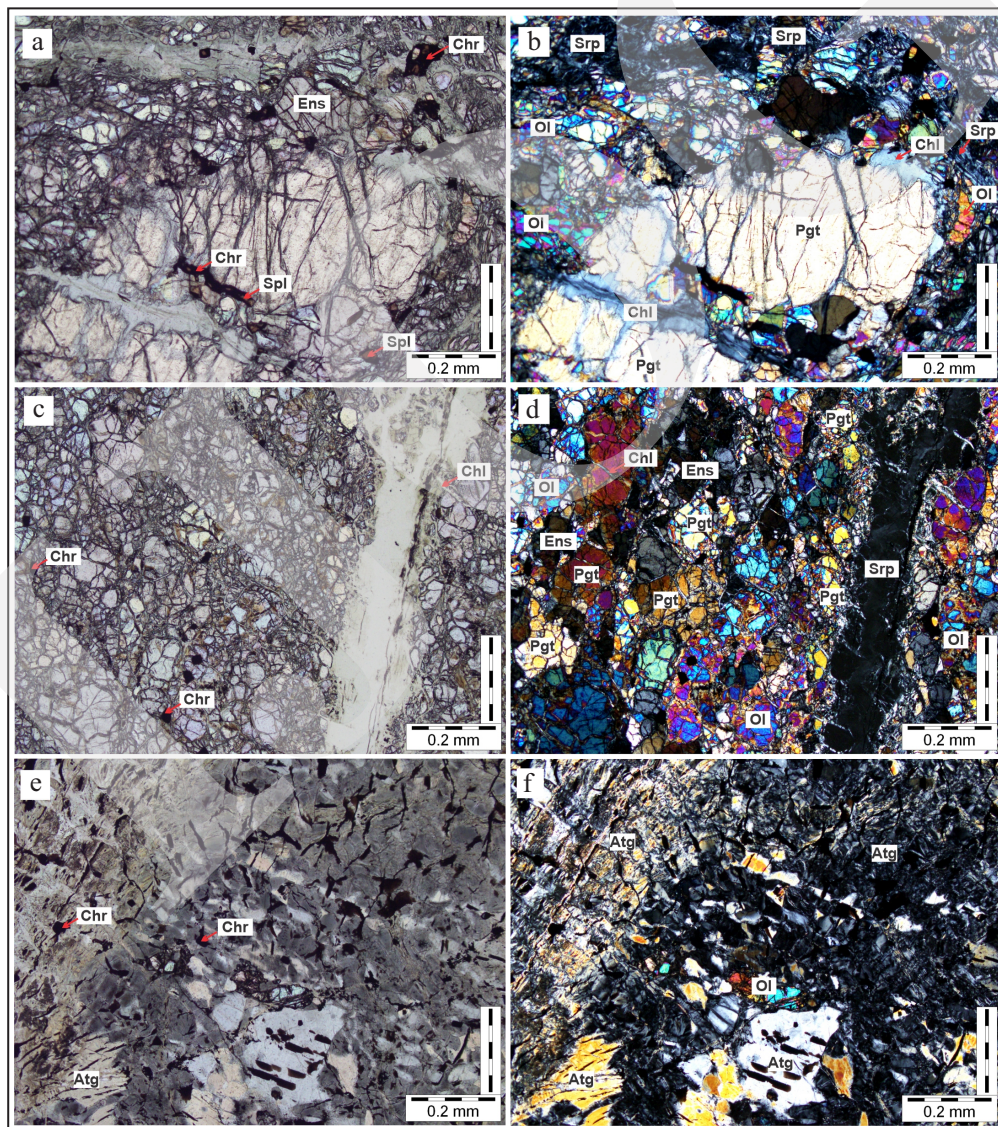

Figure 2. Photomicrographs of parallel (a,c,e) and cross (b,d,f) polarized microscope of parent rock. a-b) Rock sample from L1, and c-d) Rock sample from L2 consisting of pigeonite (pgt), olivine (ol), enstatite (ens), serpentine (srp), chlorite (chl), and chromite (chr); (e-f) Rock sample from L3 consisting of antigorite (atg), olivine (ol), and chromite (chr).
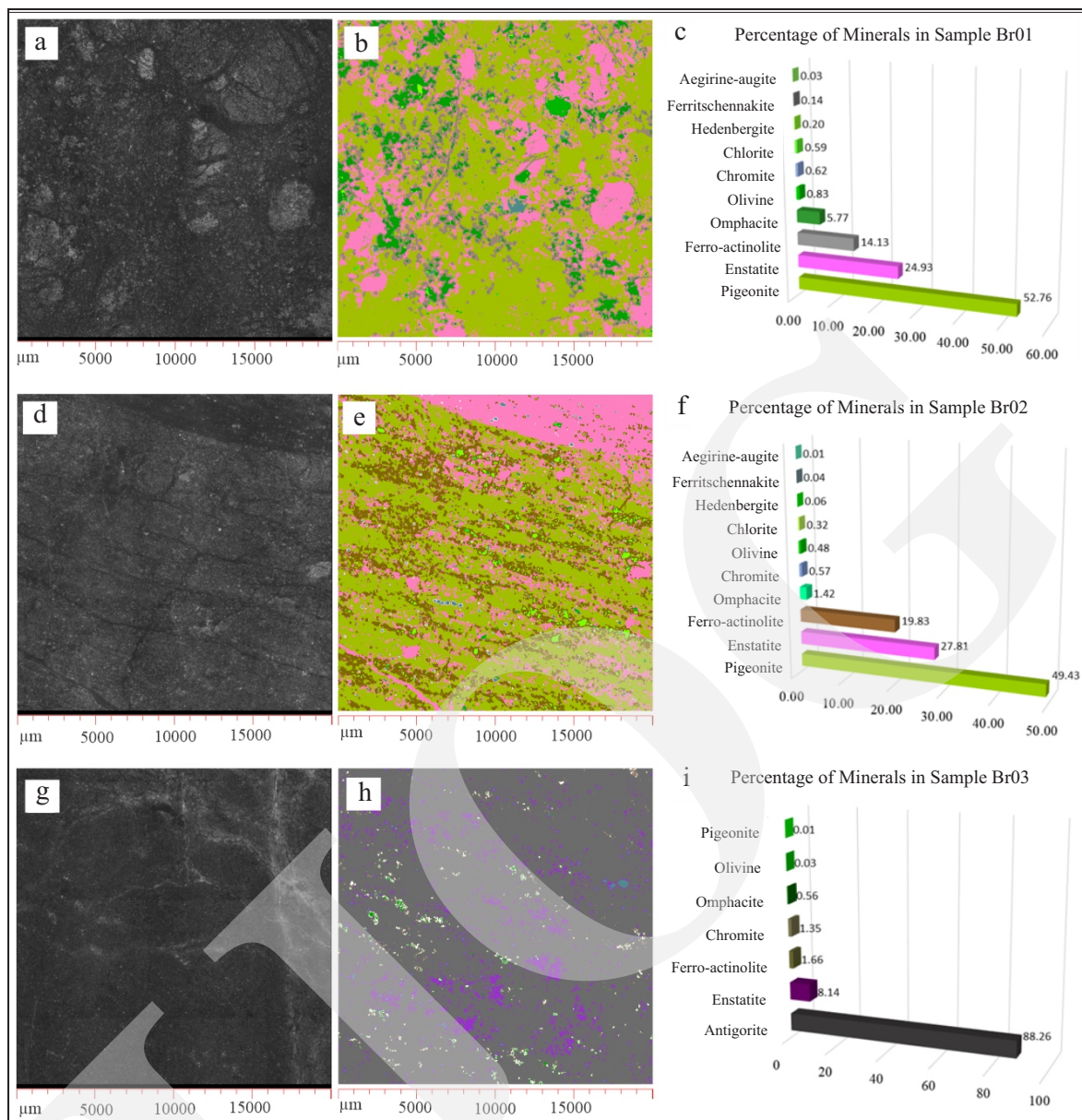
Figure 3. Back-scattered electron (BSE) images of micro-XRF analysis showing mineral distribution and percentage of minerals in parent rocks from Melati Pit. a-f) Wehrlite and g-1) Wehrlite altered to serpentinite.

a more comprehensive understanding of the diverse and intricate mineralogical composition of the parent rock material. This detailed characterization of the parent rock mineralogy lays a solid foundation for understanding the subsequent weathering and alteration processes that have ultimately shaped the formation of the Lameruru lateritic nickel deposit.

Mineralogy of Saprolitic Laterite

The saprolite zone in the studied area is composed of two distinct layers: rocky saprolite and earthy saprolite. The mineral composition of the rocky saprolite layer is characterized by the presence of maghemite, trevorite, fayalite, and chromite (Figures 4a,b,c). These mineral phases suggest a more advanced stage of weathering and alteration of the parent rock. In contrast, the earthy saprolite layer exhibits a more diverse mineral assemblage, including fayalite, chromite, trevorite, maghemite, goethite, and lizardite (Figures 4d,e,f). The presence of goethite and lizardite in this layer indicates an advanced stage of lateritization. The variation in mineral com-
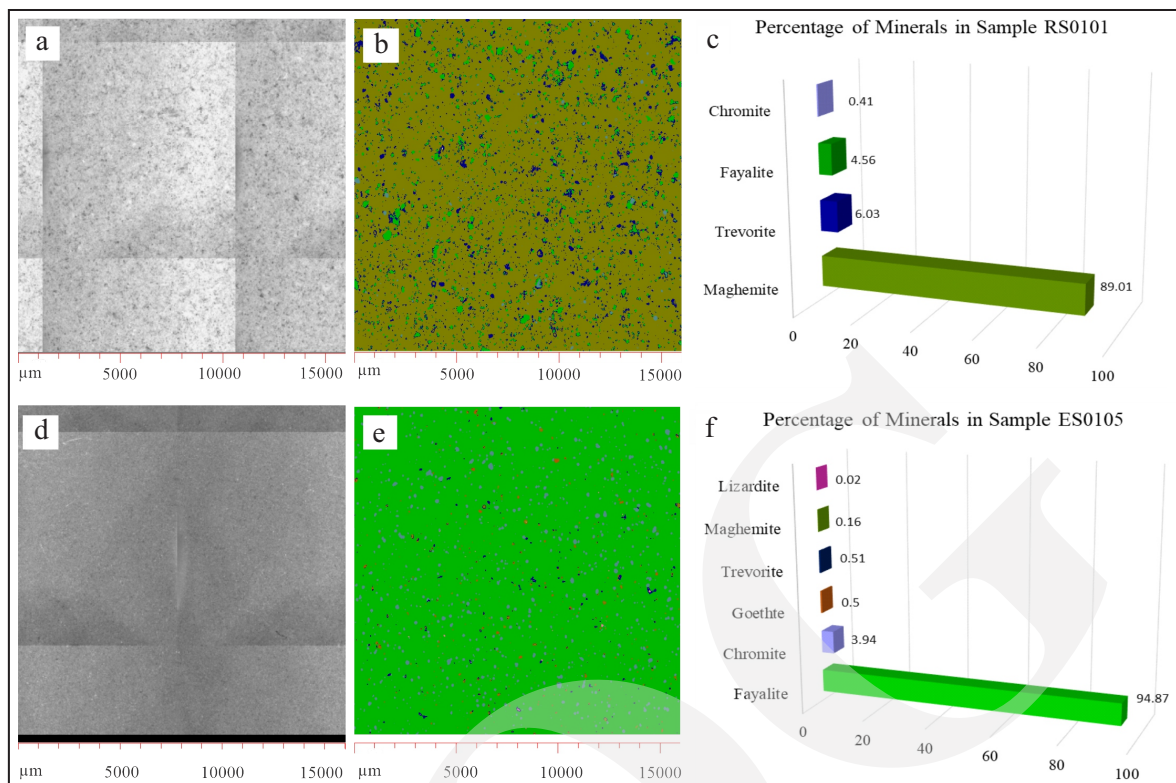
Figure 4. BSE images of micro-XRF analysis showing the mineral distribution and percentage of minerals in lateritic zone from Melati Pit. a,b,c) Rocky saprolite; d,e,f) Earthy saprolite.

position between the rocky and earthy saprolite layers reflects a gradual and complex process of weathering and alteration that has transformed the underlying ultramafic parent rock into the lateritic nickel deposit.

Mineralogy of Limonitic Laterite

The limonitic laterite zone in the studied area is further divided into two distinct sublayers including yellow limonite and red limonite, which exhibit unique mineralogical characteristics. The yellow limonite layer is primarily composed of iron oxide-hydroxide mineral goethite, which makes up the bulk of the mineral content, along with accessory chromite and nickel-bearing oxide mineral of trevorite (Figures 5a,b,c). These nickel-bearing minerals contribute significantly to the economic potential of the yellow limonite layer, as they represent the dominant hosts for economically valuable nickel. In contrast, the red limonite sublayer is dominated by the iron oxide-hydroxide goethite as the dominant

mineral constituent, accompanied by chromite as an additional mineral phase (Figures 5d,e,f). The variation in mineral assemblages between the yellow and red limonite layers reflects the progressive and complex nature of the lateritization process that has transformed the underlying ultramafic parent rock into the Lameruru lateritic nickel deposit. These mineral phases can be more readily extracted and processed for the recovery of nickel compared to the red limonite layer, which is relatively less enriched in nickel-bearing minerals.

Whole Rock Geochemistry

The analysis reveals that the highest nickel content in the earthy saprolite layer was 1.93 %, while the highest scandium content was 89.16 ppm (Table 2). This indicates a significant enrichment of nickel and scandium within the red limonite horizon, which represents the advanced stage of lateritization and weathering of the underlying ultramafic parent rock.
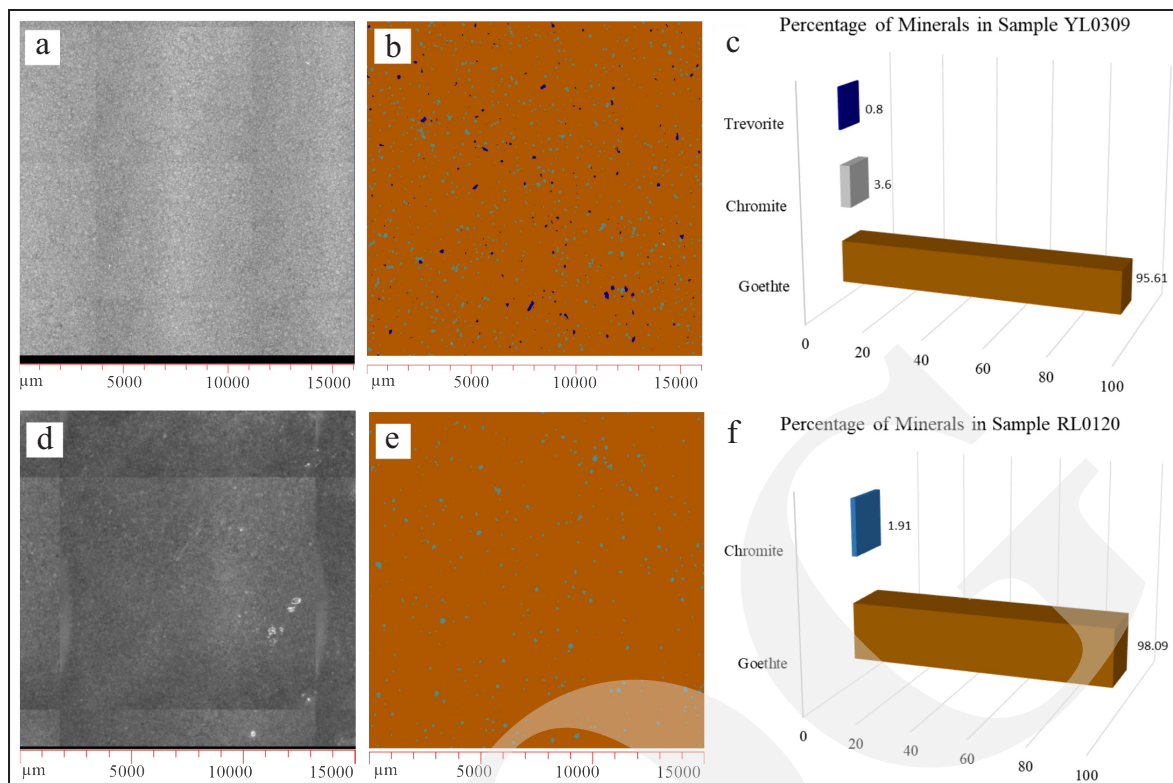
Figure 5. BSE images of micro-XRF analysis showing mineral distribution and percentage of minerals in limonitic zone from Melati Pit. a,b,c) Yellow limonite; and d,e,f) Red limonite.

A detailed geochemical profile of the nickel laterite deposit, established through comprehensive XRF and ICP-MS analyses, provides a comprehensive understanding of the transformation process from the parent peridotite rock to the final limonitic laterite. This profile illustrates a general overview progressive and complex nature of the lateritization process or the transformation of the parent rock, specifically wehrlite into limonite within the studied area (Figure 6); wherein the parent ultramafic rock undergoes extensive chemical weathering and alteration, leading to the concentration of valuable metals like nickel and scandium within the different laterite horizons.

The similarity of Fe_2O_3, MnO, and Sc patterns shows that all of them have similar geochemical behaviour during the lateritization process.

Ni-Sc-Bearing Mineral Phases
Parent Rocks

The EPMA analysis of the parent rock samples provides detailed insights into the mineral composition, including the concentrations of major oxides and Ni-Sc elements in the minerals that form the parent rock (wehrlite).

The results of this comprehensive analyses are compiled in Table 3, offering a comprehensive characterization of the mineralogical makeup of the parent material. Furthermore, the distribution of metal elements within the parent rock samples, as illustrated in Figures 7 and 8 shows spatial distribution and partitioning of these elements among the various mineral phases. The nickel is present in clinopyroxene (pigeonite, omphacite, and augite), because Ni can substitute for other transition metals, primarily Fe^{2+} and Mg^{2+}, within the clinopyroxene crystal structure. Whilst the presence or absence of scandium in clinopyroxene is a complex function of the initial magma composition, the crystallization sequence, the presence of competing minerals, and any post-crystallization processes that may have affected the rock (Orberger and Ent, 2019; Ulrich *et al*., 2018;

Nickel and Scandium-Bearing Minerals Associated with Limonitic Laterite Zone of the Lameruru Deposit in Southeast Sulawesi, Indonesia (J.M. Supit *et al.*)

Table 2. Concentrations of Major Oxide, Minor Element, and Trace Element

	RL020120	RL020119	RL020117	ES020113	ES020105	RS020101	PR0201	RL020206	RL020205	RL020201	PR0202
wt. %											
SiO_2	33.287	14.568	27.572	0.299	36.665	40.351	40.576	14.883	5.070	9.117	42.014
Al_2O_3	3.172	13.148	11.057	12.423	1.318	1.015	1.644	15.007	3.623	2.468	0.380
Fe_2O_3	49.500	52.255	43.783	0.408	34.565	8.638	8.381	50.631	72.869	70.386	7.060
MnO	0.472	0.242	0.414	0.127	0.495	0.069	0.069	0.544	2.241	<0.01	0.110
MgO	1.510	2.550	2.361	0.230	12.826	35.757	37.304	0.260	0.575	0.454	39.662
CaO	0.185	0.197	0.197	0.763	0.354	0.376	1.486	<0.01	0.033	0.032	1.044
Na_2O	0.084	0.063	0.126	0.026	0.076	0.242	0.494	0.281	0.281	0.281	0.290
TiO_2	0.077	0.494	0.504	2.264	0.090	0.077	0.066	0.015	0.132	0.011	0.013
Cr_2O_3	1.333	1.512	1.310	9.940	0.948	0.123	0.358	1.077	0.936	2.035	0.132
Co	0.048	0.027	0.044	0.299	0.034	0.014	0.009	0.069	0.427	0.662	0.013
Ni	0.947	0.771	0.968	1.242	1.929	1.191	0.244	1.083	1.284	1.356	0.259
LOI	8.954	14.015	11.291	0.408	10.070	12.026	8.915	16.100	12.500	13.200	8.930
ppm											
As	1.116	1.162	1.034	0.539	0.289	0.160	0.208	0.753	3.464	4.029	0.118
Ba	6.599	6.777	19.216	17.704	17.447	4.832	3.073	4.372	76.746	28.425	0.386
Cr	0.912	1.035	0.897	0.522	0.649	0.103	0.245	6,870.519	6,341.978	14,262.459	785.684
Cu	80.124	130.527	124.215	71.260	10.740	11.101	27.192	160.169	89.786	165.567	7.032
Ga	3.792	13.407	11.559	6.013	2.063	1.152	1.672	8.865	5.944	5.816	0.363
Hf	0.070	0.787	0.804	0.359	<0.001	0.054	0.113	0.653	0.325	0.313	0.004
Mo	0.200	0.369	0.238	0.168	0.087	0.153	0.288	0.017	0.235	0.012	0.103
Nb	0.046	0.182	0.076	0.069	<0.001	0.449	0.258	0.077	0.129	0.076	0.090
Pb	<0.001	0.667	<0.001	<0.001	<0.001	<0.001	<0.001	1.630	5.361	2.370	0.838
Rb	0.189	0.158	0.473	0.739	0.425	0.264	0.478	0.023	0.142	0.252	0.132
Sc	41.612	83.001	68.796	37.054	26.225	8.563	10.615	73.342	60.315	60.203	7.820
Sr	8.600	9.054	9.228	10.056	8.840	8.896	11.718	0.320	0.914	1.814	0.693
Ta	0.018	0.078	0.048	0.015	<0.001	0.174	0.100	0.083	0.090	0.114	0.032
Th	0.334	0.413	0.449	0.273	0.287	0.558	1.286	0.164	0.315	0.232	0.408
U	0.025	0.075	0.018	0.018	0.014	0.016	0.055	0.031	0.094	0.021	0.023
V	149.613	249.315	178.534	120.633	58.839	30.890	48.674	187.658	157.503	191.433	21.822
W	0.574	<0.002	0.042	<0.002	<0.002	0.037	<0.002	0.680	0.942	0.968	37.642
Y	1.981	5.101	93.150	13.114	1.090	0.878	2.436	4.659	104.224	184.985	0.567
Zn	137.995	120.729	120.012	196.997	121.813	26.122	32.335	159.289	589.493	682.440	26.118
Zr	1.979	15.884	13.137	7.122	0.311	1.138	2.261	13.022	4.684	0.998	0.319
La	0.597	0.910	23.000	0.900	0.782	0.346	2.613	0.619	17.038	29.226	0.780
Ce	2.239	2.990	10.193	0.923	1.535	0.775	4.655	2.842	7.427	7.725	1.596
Pr	0.162	0.282	6.546	0.233	0.160	0.090	0.532	0.304	17.678	27.680	0.183
Nd	0.761	1.371	31.376	1.304	0.573	0.319	1.884	1.345	77.027	135.273	0.579
Sm	0.296	0.520	8.703	0.510	0.107	0.070	0.392	0.617	26.198	28.671	0.120
Eu	0.097	0.169	2.818	0.219	0.031	0.021	0.054	0.203	7.976	9.648	0.002
Gd	0.102	0.209	2.871	0.221	0.048	0.038	0.170	0.159	7.327	12.838	<0.001
Tb	0.028	0.061	0.891	0.076	0.006	0.009	0.034	0.083	2.667	4.032	0.008
Dy	0.314	0.659	9.843	0.961	0.067	0.096	0.328	0.923	28.668	47.311	0.078
Ho	0.074	0.170	2.601	0.267	0.016	0.022	0.079	0.206	6.252	11.514	0.014
Er	0.232	0.514	7.568	0.838	0.074	0.079	0.228	0.666	17.705	34.427	0.050
Tm	0.037	0.076	1.068	0.119	0.007	0.009	0.031	0.104	2.530	4.722	0.004
Yb	0.428	0.729	8.482	0.957	0.113	0.114	0.296	0.857	17.479	32.783	0.079
Lu	0.052	0.090	1.090	0.129	0.014	0.013	0.033	0.132	2.754	5.803	0.008
Total (wt. %)	99.568	99.840	99.629	99.579	99.371	99.879	99.546	99.949	99.970	100.002	99.907
Total REE (ppm)	5.418	8.750	117.050	7.656	3.534	2.001	11.330	9.060	38.726	391.653	3.501

PR (parent rock), RS (rocky saprolite), ES (earthy saprolite), YL (yellow limonite), dan RL (red limonite).

Continued Table 2. Concentrations of Major Oxide, Minor Element, and Trace Element

	RL020323	RL020321	YL020318	YL020312	YL020309	ES020308	ES020305	RS020301	PR0203
wt. %									
SiO_2	12.285	16.103	8.597	14.306	13.126	44.873	49.676	51.080	34.897
Al_2O_3	15.744	14.798	12.595	10.179	2.197	8.963	5.052	6.402	0.249
Fe_2O_3	52.577	50.341	58.899	56.376	70.340	28.505	18.006	20.658	8.056
MnO	0.341	0.341	0.489	1.039	0.947	0.458	0.307	0.293	0.106
MgO	0.178	0.253	0.152	1.382	0.588	3.862	14.513	9.123	38.913
CaO	<0.01	<0.01	<0.01	<0.01	0.035	0.064	0.516	0.297	0.301
Na_2O	0.284	0.262	0.258	0.269	0.259	0.240	0.242	0.251	0.316
TiO_2	0.543	0.015	0.016	0.285	0.019	0.303	0.159	<0,01	<0.01
Cr_2O_3	1.310	1.306	1.546	1.829	0.402	1.042	0.582	0.703	0.082
Co	0.029	0.029	0.048	0.100	0.089	0.038	0.023	0.024	0.011
Ni	0.903	0.897	1.002	0.920	1.828	1.256	1.009	1.139	0.242
LOI	15.800	15.600	16.400	13.200	10.200	10.300	10.000	10.060	16.800
ppm									
As	2.444	1.563	0.619	1.829	1.402	0.704	0.271	0.440	0.034
Ba	2.016	2.989	3.852	13.850	26.964	19.633	18.154	14.372	0.307
Cr	9,226.138	8,456.761	10,512.389	12,166.702	2,501.684	6887.742	3988.325	4727.345	568.183
Cu	134.539	138.771	202.997	230.504	48.046	79.441	47.861	60.403	4.340
Ga	10.494	9.526	10.072	8.948	3.991	7.485	3.883	5.165	0.343
Hf	0.806	0.710	0.726	0.408	0.082	0.325	0.192	0.254	0.001
Mo	0.193	0.092	0.020	0.284	0.035	<0.002	<0.002	<0.002	0.062
Nb	0.351	0.258	0.166	0.193	0.052	0.097	0.006	0.046	0.193
Pb	5.058	2.513	0.761	0.982	0.587	0.395	0.396	1.208	0.617
Rb	0.026	0.063	0.045	0.097	0.099	0.168	0.592	0.877	0.080
Sc	71.177	82.881	89.158	67.698	41.821	45.629	28.507	34.925	7.469
Sr	0.745	0.585	0.317	0.844	0.720	1.221	1.542	1.998	0.427
Ta	0.147	0.139	0.142	0.195	0.072	0.046	0.015	0.047	0.079
Th	0.471	0.451	0.102	0.196	0.048	0.597	0.029	0.122	0.225
U	0.207	0.117	0.032	0.034	0.008	0.029	<0.001	0.008	<0.001
V	301.762	273.794	326.914	328.272	183.553	121.869	69.300	66.182	15.611
W	0.481	0.015	0.770	0.126	0.718	0.148	4.597	0.968	1.647
Y	4.787	4.979	9.730	79.732	117.743	33.906	5.246	8.627	0.200
Zn	189.395	153.550	181.203	455.387	585.699	376.859	67.423	153.600	36.557
Zr	18.828	16.071	14.846	6.200	0.405	6.210	3.523	4.795	0.208
La	0.633	0.808	1.005	10.805	18.467	7.139	0.305	0.675	0.662
Ce	3.151	4.621	3.761	5.478	0.399	3.414	0.592	0.987	0.720
Pr	0.227	0.306	0.544	6.384	5.580	1.543	0.121	0.199	0.078
Nd	1.029	1.300	2.416	28.312	24.414	6.382	0.640	0.960	0.279
Sm	0.462	0.555	1.284	12.452	7.609	1.746	0.332	0.412	0.045
Eu	0.168	0.205	0.470	4.290	2.934	0.591	0.157	0.166	<0.005
Gd	0.132	0.180	0.388	3.728	3.209	0.669	0.060	0.089	<0.001
Tb	0.071	0.079	0.188	1.550	1.127	0.224	0.048	0.060	0.002
Dy	0.877	0.931	2.359	17.848	12.831	2.547	0.608	0.717	0.030
Ho	0.210	0.218	0.548	3.964	3.147	0.653	0.145	0.183	0.003
Er	0.708	0.713	1.855	12.386	9.122	1.893	0.463	0.571	0.016
Tm	0.113	0.115	0.323	2.015	1.179	0.244	0.064	0.083	<0.005
Yb	0.908	0.974	2.889	15.478	7.573	1.663	0.502	0.609	0.024
Lu	0.151	0.160	0.452	2.435	1.245	0.258	0.077	0.099	<0.005
Total (wt. %)	99.993	99.945	100.002	99.886	100.030	99.904	100.086	100.031	99.973
Total REE (ppm)	8.840	11.166	18.483	127.125	98.836	28.966	4.116	5.813	1.858

PR (parent rock), RS (rocky saprolite), ES (earthy saprolite), YL (yellow limonite), dan RL (red limonite).
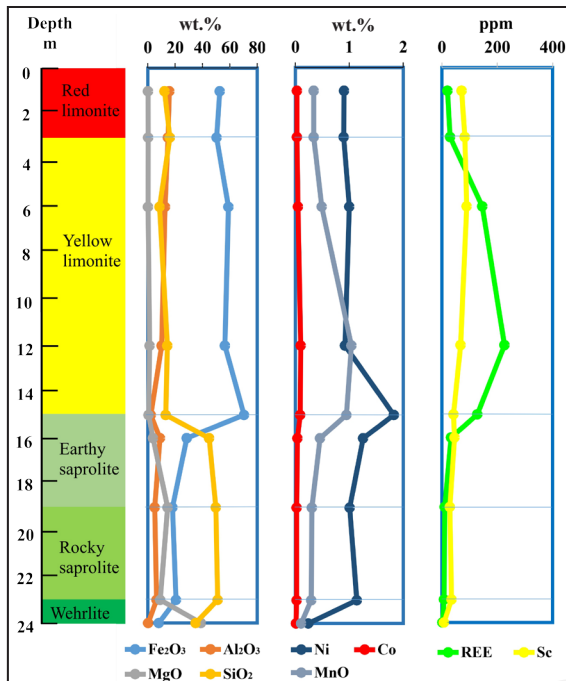
Figure 6. Geochemical profile of the nickel laterite deposit at the studied area. Major oxide and minor element compositions are shown in wt. %, whereas scandium and REE are shown in ppm.

Williams-Jones and Vasyukova, 2018; Chassé *et al*., 2016).

Rocky Saprolite

The EPMA analysis of the rocky saprolite zone, which represents the weathered and altered product of the wehrlite parent rock, reveals the composition of major oxides, minor elements, and

trace elements in the mineral assemblage derived from the lateritization process.

The comprehensive analytical results of the mineral chemistry are compiled in Table 4, which offer a comprehensive characterization of the mineralogical content of the parent rock samples. Furthermore, the distribution of metal elements within the rocky saprolite samples, as illustrated in Figures 9 and 10, shows the spatial distribution and partitioning of these elements among the various mineral phases. The nickel is present in willemseite with silica, because nickel becomes incorporated into willemseite, while the silica precipitates. These nickel-bearing minerals and Silica minerals can occur as intergrowths, vein fillings, or coatings on each other (Xiao *et al*., 2021; Butt and Wang, 2013). The presence of scandium in willemseite depends on the availability of scandium during its formation and competition with other elements for inclusion in its structure. Silica minerals, on the other hand, do not readily incorporate scandium into their crystal structures, so most likely the presence of scandium in silica is due to surface adsorption (Wang *et al.,* 2020).

Earthy Saprolite

The EPMA analysis of the earthy saprolite zone, which represents the advanced weathered

Table 3. EPMA Analysis Results Showing the Concentrations of Major Oxides, Ni, and Sc in Several Key Minerals of the Parent Rock (wehrlite)

| Mineral	Pigeonite	Omphacite	Augite	Augite	Augite
Major Oxide	Point_1	Point_2	Point_3	Point_4	Point_5
	wt. %	wt. %	wt. %	wt. %	wt. %
CaO	21.946	11.770	0.677	0.655	0.617
Cr_2O_3	0.783	1.247	0.458	0.481	0.533
SiO_2	52.111	42.698	54.728	54.678	54.845
Al_2O_3	5.762	14.725	4.521	4.312	4.357
Na_2O	1.190	3.380	0.630	0.038	0.046
MgO	15.080	16.612	31.663	31.677	32.274
TiO_2	0.345	2.383	0.112	0.044	0.016
FeO	2.443	3.550	6.086	6.124	6.211
Total	99.660	96.365	98.875	98.009	98.899
Elements					
Ni	0.040	0.050	0.037	0.044	0.029
Sc	0.012	0.068	0.000	0.000	0.023
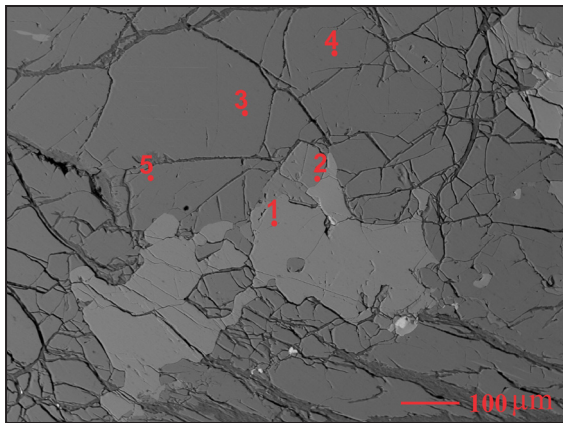
Figure 7. EPMA back-scattered image showing the occurrence of pigeonite (point 1), omphacite (point 2), and augite (points 3, 4, 5) in the parent rock specimen.

and altered product of the rocky saprolite, revealed the composition of major oxides, minor elements, and trace elements in the mineral assemblage derived from the lateritization process.

The comprehensive analytical results of the mineral chemistry are compiled in Table 5, which offer a comprehensive characterization of the mineralogical makeup of the rocky saprolite. Furthermore, the distribution of metal elements within the earthy saprolite samples, as illustrated in Figures 11 and 12, displays the spatial distribution and partitioning of these elements among the various mineral phases. The nickel is present in vermiculite, lizardite, and antigorite, because all
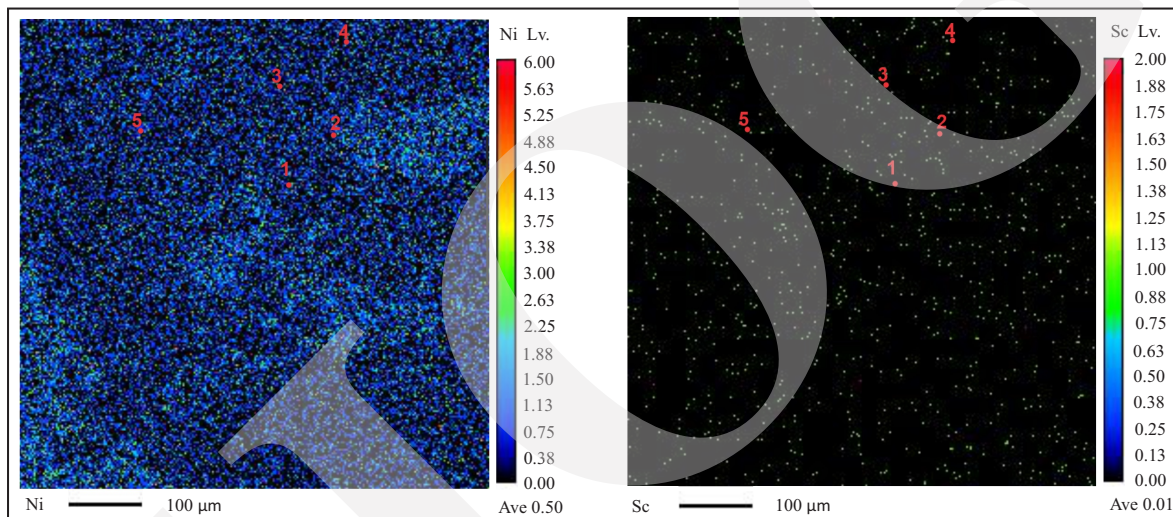
Figure 8. Elemental mapping results of Ni and Sc in the parent rock sample. 1) Pigeonite with 0.040 % Ni, 0.012 % Sc; 2) Omphacite with 0.050 % Ni, 0.068 % Sc; 3) Augite with 0.037 % Ni; 4) Augite with 0.044 % Ni; 5) Augite with 0.029 % Ni, 0.023 % Sc.

Table 4. EPMA Analysis Results Showing the Concentrations of Major Oxides, Ni, And Sc in Several Key Minerals of the Rocky Saprolite

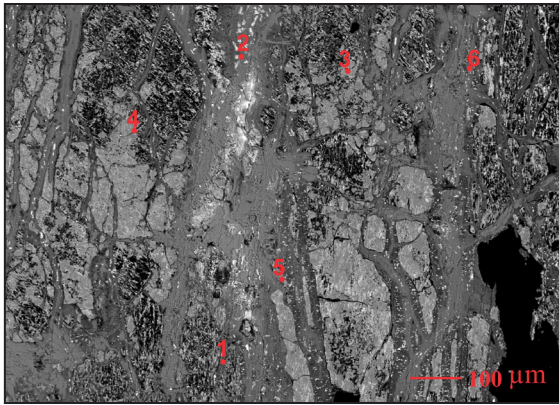| Mineral	Willemseite	Willemseite	Silica	Silica	Silica	Willemseite
Major Oxide	Point_1	Point_2	Point_3	Point_4	Point_5	Point_6
	wt. %	wt. %	wt. %	wt. %	wt. %	wt. %
CaO	0.020	0.004	0.001	0.005	0.006	0.010
Cr_2O_3	0.027	0.022	0.088	0.039	0.032	0.024
SiO_2	32.557	28.374	64.129	89.625	79.580	33.152
Al_2O_3	0.860	1.569	0.491	0.105	0.183	1.384
Na_2O	0.002	0.000	0.002	0.000	0.018	0.016
MgO	25.460	16.859	0.532	0.267	6.831	23.553
TiO_2	0.028	0.008	0.023	0.000	0.008	0.016
FeO	3.662	4.367	17.089	4.929	5.270	4.752
Total	62.616	51.203	82.355	94.970	91.928	62.907
Elements						
Ni	13.641	20.805	2.089	0.778	0.848	20.528
Sc	0.000	0.026	0.000	0.010	0.000	0.061

Figure 9. EPMA back-scattered image showing the occurrence of willemseite (points 1, 2, 6), and silica (point 3, 4, 5) in the rocky saprolite specimen.

of them are phyllosilicate minerals, meaning they have a layering structure. Nickel can substitute for magnesium or iron within the octahedral sheet of these minerals. Lizardite and antigorite are both forms of serpentine, a common alteration product of olivine and pyroxene in ultramafic rocks. Nickel is often present in olivine, and during serpentinization, this nickel can be incorporated into the newly formed serpentine minerals (Muñoz *et al.*, 2018). While nickel is present in maghemite, because during lateritization, nickel can be released from weathering primary minerals and become adsorbed onto the surfaces of iron oxides like
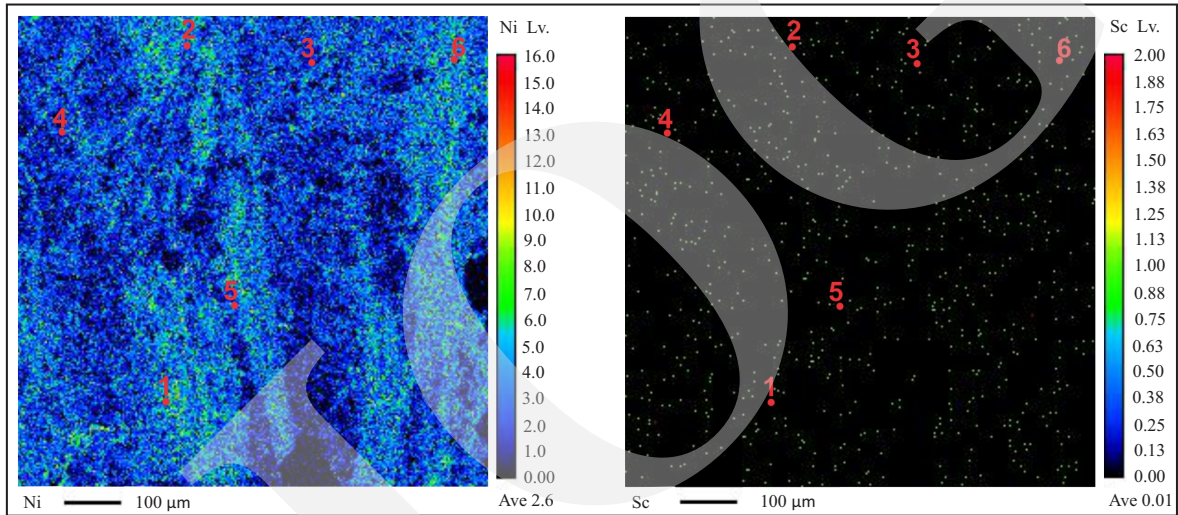
Figure 10. Elemental mapping results of Ni and Sc in the rocky saprolite sample. 1) Willemseite with 13.641 % Ni; 2) Willemseite with 20.805 % Ni, 0,026 % Sc; 3) Silica with 2.089 % Ni; 4) Silica 0.0778 % Ni, 0,010 % Sc; 5) Silica with 0.848 % Ni; 6) Willemseite with 20.528 % Ni, 0.061 % Sc.

Table 5. EPMA Analysis Results Showing the Concentrations of Major Oxides, Ni, And Sc in Several Key Minerals of the Earthy Saprolite

| Mine-rals	Vermiculite	Vermiculite	Lizardite	Vermiculite	Vermiculite	Lizardite	Maghemite	Antigorite
Major Oxide	Point_1	Point_2	Point_3	Point_4	Point_5	Point_6	Point_7	Point_8
	wt .%	wt. %	wt. %	wt. %	wt. %	wt. % t	wt. %	wt. %
CaO	0.037	0.000	11.723	0.064	0.005	0.045	0.000	0.057
Cr_2O_3	0.688	0.790	0.195	0.182	1.441	0.524	2.140	0.596
SiO_2	24.337	25.294	53.466	26.290	22.540	37.022	8.579	31.924
Al_2O_3	5.134	6.853	0.609	4.900	5.005	7.286	3.258	6.289
Na_2O	0.000	0.019	0.116	0.011	0.051	0.024	0.016	0.029
MgO	7.943	14.420	20.753	9.793	13.444	18.400	0.855	15.759
TiO_2	0.109	0.000	0.053	0.091	0.236	0.040	0.816	0.103
FeO	9.483	8.844	2.465	6.499	19.572	8.044	34.333	7.826
Total	57.671	56.220	89.380	47.830	62.294	71.385	49.997	62.583
Elements								
Ni	24.683	20.476	0.786	34.153	6.277	29.479	11.709	31.727
Sc	0.029	0.000	0.034	0.027	0.077	0.000	0.000	0.000
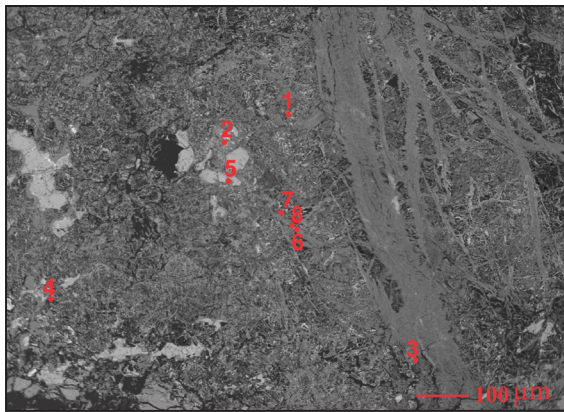
Figure 11. EPMA back-scattered image showing the occurrence of vermiculite (points 1,2,4,5), lizardite (points 3,6), maghemite (point 7), and antigorite (point 8) in the earthy saprolite specimen.

maghemite (Butt and Wang, 2013). The presence or absence of scandium, in vermiculite, lizardite, maghemite, and antigorite depends on several factors, including the mineral structure, its surrounding geochemical environment during formation, and subsequent alteration processes (Chassé *et al*., 2016; Ulrich *et al*., 2018; Wang *et al*., 2020).

Yellow Limonite

The EPMA analysis of the yellow limonite zone, which represents the advanced weathered and altered product of the earthy saprolite, re-

vealed the composition of major oxides, minor elements, and trace elements in the mineral assemblage derived from the lateritization process.

The comprehensive analytical results of the mineral chemistry are compiled in Table 6, which offer a comprehensive characterization of the mineralogical composition of the earthy saprolite. Furthermore, the distribution of metal elements within the yellow limonite samples, as illustrated in Figures 13 and 14, displays the spatial distribution and partitioning of these elements among the various mineral phases. The nickel is present in goethite, because nickel can substitute iron within the goethite structure. Goethite is an iron oxyhydroxide (FeO), and nickel can replace some of the iron in the crystal lattice due to their similar ionic radii and charges (Tauler *et al*., 2023). This substitution likely occurs during goethite formation, when nickel is present in the surrounding fluids. The presence and concentration of scandium in goethite depend on complex factors such as scandium availability, surface area, pH, and Eh conditions and competition with other elements (Chassé *et al*., 2016; Teitler *et al*., 2018; Qin *et al*., 2020).

Red Limonite

The EPMA analysis of the red limonite zone, which represents the advance weathered and al-
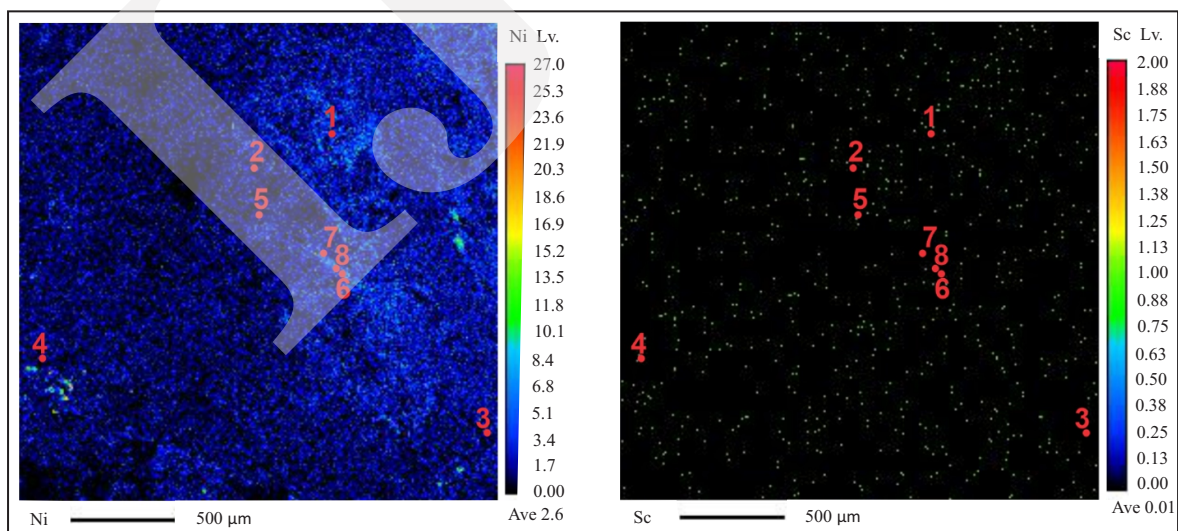

Figure 12. Elemental mapping results of Ni and Sc in the earthy saprolite sample. 1) Vermiculite with 24.683 % Ni, 0.029 % Sc; 2) Vermiculite with 20.476 % Ni. 3) Lizardite with 0.786 % Ni, 0.034 % Sc; 4) Vermiculite with 34.153 % Ni, 0.027 % Sc; 5) Vermiculite with 6.277 % Ni, 0.077 % Sc; 6) Lizardite with 29.479 % Ni. 7) Maghemite with 11.709 % Ni. 8) Antigorite with 31.727 % Ni.

Table 6. EPMA Analysis Results Showing the Concentrations of Major Oxides, Ni, And Sc in Several Key Minerals of the Yellow Limonite

Minerals	Goethite	Goethite	Goethite
Major Oxide	Point_1	Point_2	Point_3
	wt. %	wt. %	wt. %
CaO	0.000	0.000	0.000
Cr_2O_3	1.380	0.892	1.415
SiO_2	1.434	1.337	1.460
Al_2O_3	5.349	4.904	5.242
Na_2O	0.037	0.055	0.031
MgO	0.186	0.205	0.167
TiO_2	0.079	0.021	0.079
FeO	41.531	42.054	40.356
Total	49.996	49.468	48.750
Element			
Ni	5.952	6.202	0.528
Sc	0.000	0.051	0.017
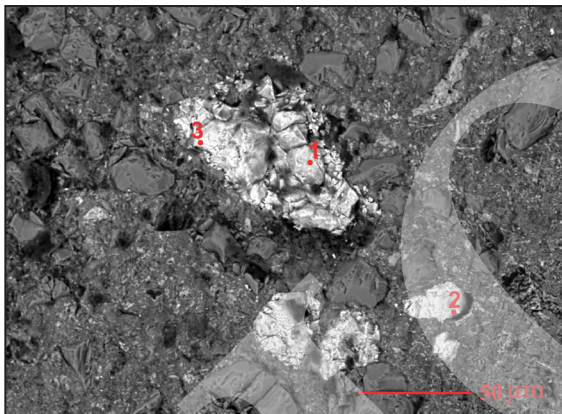
Figure 13. EPMA back-scattered image showing the occurrence of goethite (points 1, 2, 3) in the yellow limonite specimen

tered product of the yellow limonite, revealed the composition of major oxides, minor elements, and trace elements in the mineral assemblage derived from the lateritization process.

The comprehensive analytical results of the mineral chemistry are compiled in Table 7, which offer a comprehensive characterization of the mineralogical composition of the yellow limonite. Furthermore, the distribution of metal elements within the red limonite samples, as illustrated in Figures 15 and 16, shows the spatial distribution and partitioning of these elements among the various mineral phases. The scandium can be found in association with both gibbsite and kaolinite,
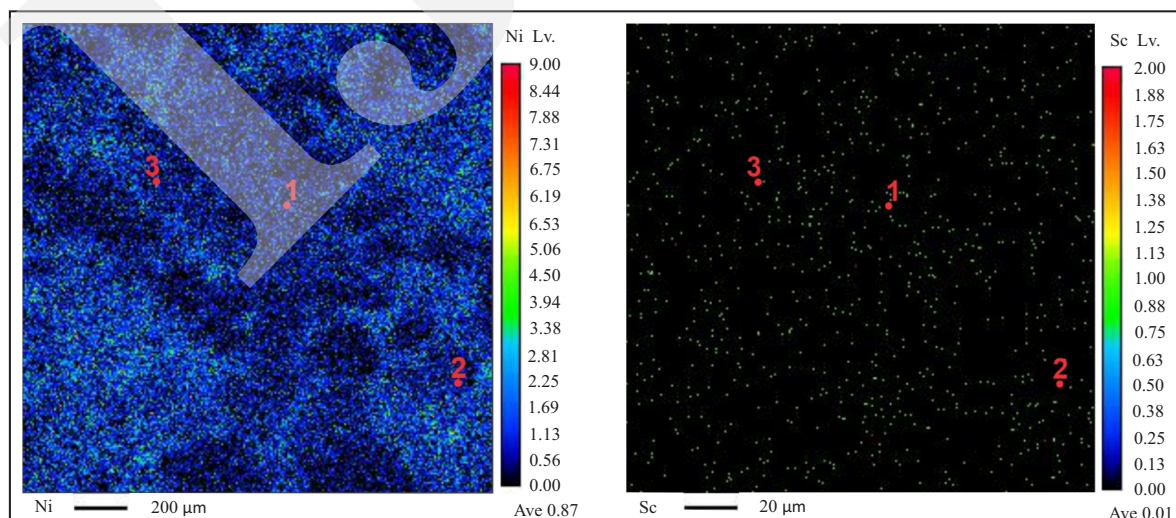

Figure 14. Elemental mapping results of Ni-Sc in alteration minerals in yellow limonite samples. 1) Goethite with 5.952 % Ni; 2) Goethite with 6.202 % Ni, 0.051 % Sc; 3) Goethite with 0.528 % Ni, 0.017 % Sc.

189

Table 7. EPMA Analysis Results Showing the Concentrations of Major Oxides, Ni, And Sc in Several Key Minerals of the Red Limonite

| Minerals	Vermiculite	Maghemite	Goethite	Kaolinite	Goethite	Gibbsite	Goethite
Major Oxide	Point_1	Point_2	Point_3	Point_4	Point_5	Point_6	Point_7
	wt. %	wt. %	wt. %	wt. %	wt. %	wt. %	wt. %
CaO	0.085	0.009	0.000	0.057	0.000	0.000	0.000
Cr_2O_3	0.266	0.180	0.095	0.135	1.504	9.902	0.381
SiO_2	28.912	1.441	3.590	36.332	6.797	0.000	0.134
Al_2O_3	15.927	3.145	7.549	26.173	5.802	53.531	0.009
Na_2O	0.000	0.031	0.006	0.009	0.027	0.000	0.006
MgO	0.834	0.512	0.000	3.130	0.383	16.908	0.318
TiO_2	0.228	0.017	0.092	0.114	0.068	0.075	0.076
FeO	0.085	31.157	62.360	6.877	58.506	14.805	94.420
Total	59.350	36.492	73.692	72.827	73.087	95.221	95.344
Elements							
Ni	4.036	6.962	5.710	2.626	7.320	1.687	0.000
Sc	0.000	0.018	0.000	0.017	0.100	0.034	0.025
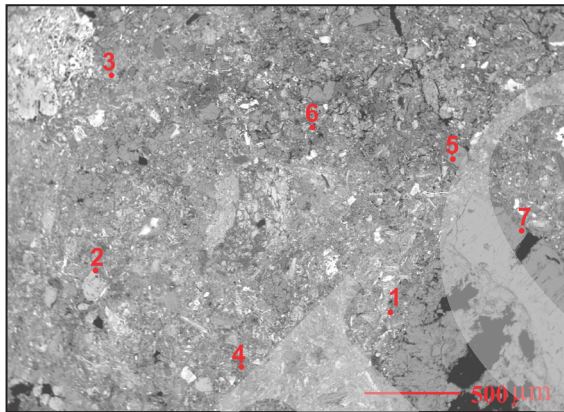
Figure 15. EPMA back-scattered image showing the occurrence of vermiculite (point 1), maghemite (point 2), goethite (points 3,5,7), kaolinite (point 4), and gibbsite (points 6) in the red limonite specimen.

although the mechanisms differ. Limited substitution might occur in gibbsite, but adsorption is more common for both minerals. The specific conditions during mineral formation and subsequent alteration processes play a crucial role in determining the presence and concentration of scandium in these minerals (Chassé *et al*., 2016; Qin *et al*., 2020).

Discussion

Ultramafic Rock Composition

The ultramafic rocks, as the parent rock of the lateritic nickel deposit, are predominantly composed of clinopyroxene, orthopyroxene, olivine,
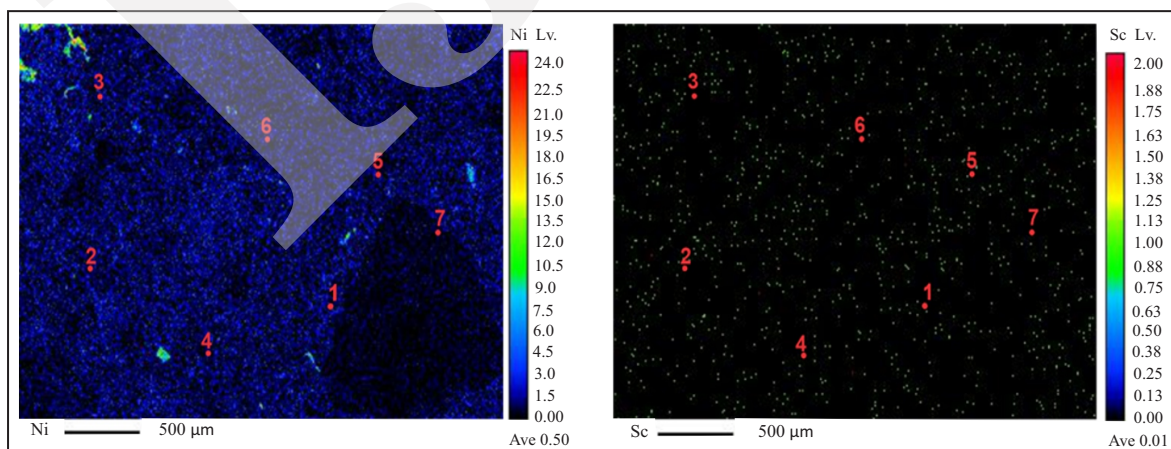

Figure 16. Elemental mapping results of Ni-Sc in alteration minerals in red limonite samples. 1) Vermiculite with 4.036 % Ni; 2) Maghemite with 6.962 % Ni, 0.018 % Sc; 3) Goethite with 5.710 % Ni. 4) Kaolinite with 2.626 % Ni, 0.017 % Sc; 5) Goethite with 7.320 % Ni, 0.100 % Sc; 6) Gibbsite with 1.687 % Ni, 0.034 % Sc; 7) Goethite with 0.025 % Sc.

and amphibole. They are the primary silicate minerals found in these igneous rocks (Garnier *et al*., 2009; Tupaz *et al*., 2020). The clinopyroxene subgroup minerals (pigeonite, augite, and omphacite), orthopyroxene subgroup mineral, such as enstatite, and then olivine subgroup minerals, such as fayalite, and amphibole subgroup minerals, such as ferro-actinolite, make up the bulk mineralogical composition of the ultramafic parent rocks. This mineral assemblage is the characteristic of peridotite suite, which includes dunite, harzburgite, and wehrlite (Garnier *et al*., 2009; Bai *et al.,* 2019; Maurizot *et al*., 2019). In Melati pit at Lameruru nickel deposit, the parent rock is wehrlite. The alteration of wehrlite forming minerals is a crucial factor governing the weathering and lateritization processes that have led to the formation of the economically valuable Ni-Sc (Garnier *et al*., 2009).

Mineral Formation in Lateritization

The intense chemical weathering associated with the lateritization process, driven by the hot and humid tropical climate, has resulted in the progressive breakdown and alteration of the primary silicate minerals, such as clinopyroxene, orthopyroxene, olivine, and amphibole (Wilson, 2004; Garnier *et al*., 2009). This weathering-driven transformation has led to the progressive transformation of the parent rock into a layered lateritic profile, with distinct horizons enriched in economically valuable minerals and metals (Ent *et al*., 2013; Fu *et al*., 2014; Maurizot *et al*., 2019). The transformation of the primary minerals making up the peridotite resulted in alteration minerals such as willemseite (garnierite group), vermiculite (clay group), lizardite and antigorite (serpentine group), maghemite, goethite, gibbsite, and kaolinite (Ent *et al*., 2013; Fu *et al*., 2014; Maurizot *et al*., 2019).

Nickel Enrichment During Lateritization

The intense chemical weathering during lateritization has driven the progressive enrichment of nickel within the different horizons of the lateritic profile. As the underlying ultramafic parent rock undergoes extensive alteration and transformation, the nickel-bearing minerals, such as garnierite, clay, serpentine, become increasingly concentrated within the various laterite layers (Butt and Wang, 2013; Fu *et al*., 2014). This selective enrichment of nickel is a result of the complex geochemical processes that selectively partition and accumulate this economically valuable metal, making the lateritic profile a valuable source of nickel ore . The geochemical processes involved in nickel enrichment during lateritization are complex and involve several stages such as weathering of parent rock, leaching and disolusion, presipitation and adsorption, vertical differentiation and role of groundwater (Li *et al*., 2012; Farrokhpay *et al.,* 2019). The presence of nickel enrichment in saprolite is due to Ni-bearing minerals such as willemseite, vermiculite, lizardite and antigorite are accumulated in saprolitic zones.

.

Scandium Concentration in Laterized Ultramafic Rock

The lateritic profile developed over the ultramafic rocks in the Lameruru area, also exhibits a significant enrichment of scandium, particularly within the limonite horizon of the lateritic profile (Fu *et al*., 2014; Maulana *et al*., 2019; Konopka *et al*., 2022). The limonite horizon represents the most advanced stage of lateritization, where the intense chemical weathering and alteration processes have led to the selective concentration and enrichment of scandium-bearing mineral phases (Chassé *et al*., 2016; Cui, 2018; Ulrich *et al*., 2018). The detailed mineralogical analysis of this horizon has revealed the presence of scandium-bearing goethite and gibbsite and small amounts of scandium-bearing kaolinite and maghemite, which act as the main host phases for critical metal (Wang *et al*., 2011; Chassé *et al*., 2 016; Sanematsu *et al*., 2017; Altinsel *et al*., 2018; Cui and Nie, 2018; Anderson, 2018). This selective partitioning and accumulation of scandium within the red limonite layer is a

testament to the complex geochemical transformations that have occurred during the lateritization of the underlying ultramafic parent rock, ultimately making this horizon a valuable source of scandium-enriched ore. This is evident from the micro-XRF results which show that at the researched location, the goethite content in red limonite is higher compared to yellow limonite or earthy and rocky saprolite (Figures 4 and 5). Thus, the EPMA results which indicate that goethite is an Sc-bearing mineral (Figures 13 and 15) further strengthen the geochemical analysis results where the Sc content is rich in red limonite zone.

Nickel and Scandium-Bearing Minerals

The detailed mineralogical analysis of laterite profiles, utilizing advanced techniques such as electron probe microanalysis, has revealed the presence and distribution of specific nickel and scandium-bearing mineral phases within the different horizons of laterite deposits (Fu *et al*., 2014; Sanematsu *et al*., 2017; Quast *et al*., 2017; Orberger and Ent, 2019; Tamehe *et al*., 2024). In the saprolite zone Ni-bearing minerals are willemseite, vermiculite, lizardite, antigorite, and maghemite, while Sc-bearing minerals are vermiculite and lizardite (Tables 4 and 5). The limonite zone Ni-bearing minerals are vermiculite, maghemite, goethite, kaolinite, and gibbsite, while Sc-bearing mineral are goethite, maghemite, kaolinite, and gibbsite (Tables 6 and 7). Based on the analysis results, Ni is contained

in almost all of the bearing minerals, while Sc is not. It is reasonable to assume that Ni is structurally bound to the bearing minerals, while Sc is adsorbed on the surface of the bearing minerals (Konopka *et al*., 2022).This comprehensive analysis has provided the valuable insight into the complex geochemical processes that have led to the selective enrichment and separation of these economically important elements among the various mineral assemblages that make up the layered laterite profile.

The geochemical conditions of the rocks and the chemical conditions of the minerals that compose them significantly influence the enrichment of Ni-Sc during the lateritization process. Ultramafic rocks reflect the characteristics of their constituent minerals, the characteristics of both will influence each other. This can be seen from the changes in Ni-Sc levels in each lateritization zone. As Ni levels increase from the parent rock zone to the earthy saprolite zone, Sc levels also tend to increase. However, from the earthy saprolite zone to the red limonite zone, Ni levels decrease, while Sc levels increase. This condition can be seen in Figure 17, which presents geochemical and mineral chemistry data as a comparison to understand Ni-Sc enrichment.

Based on the results and discussion, a relationship can be drawn between the lateritization process and the mineral composition in the lateritic zone towards the bearing minerals and Ni-Sc enrichment (Figure 18).
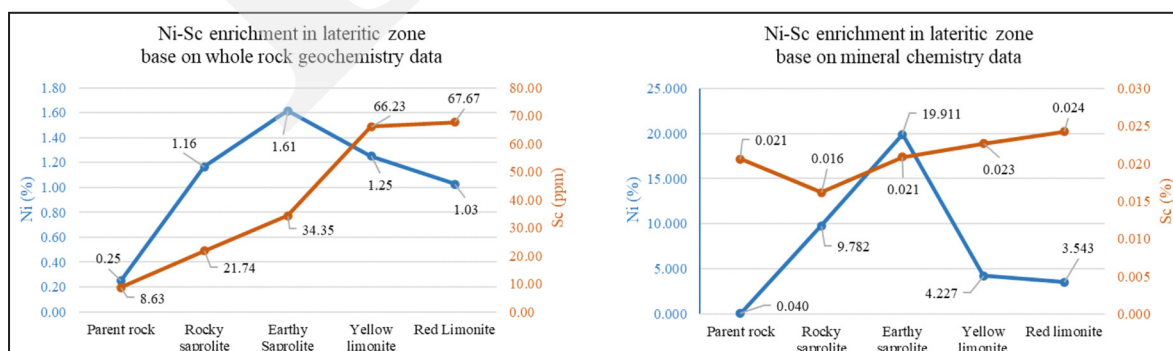

Figure 17. Comparison of Ni-Sc enrichment during lateritization based on average data of whole rock geochemistry (left) and mineral chemistry (right).
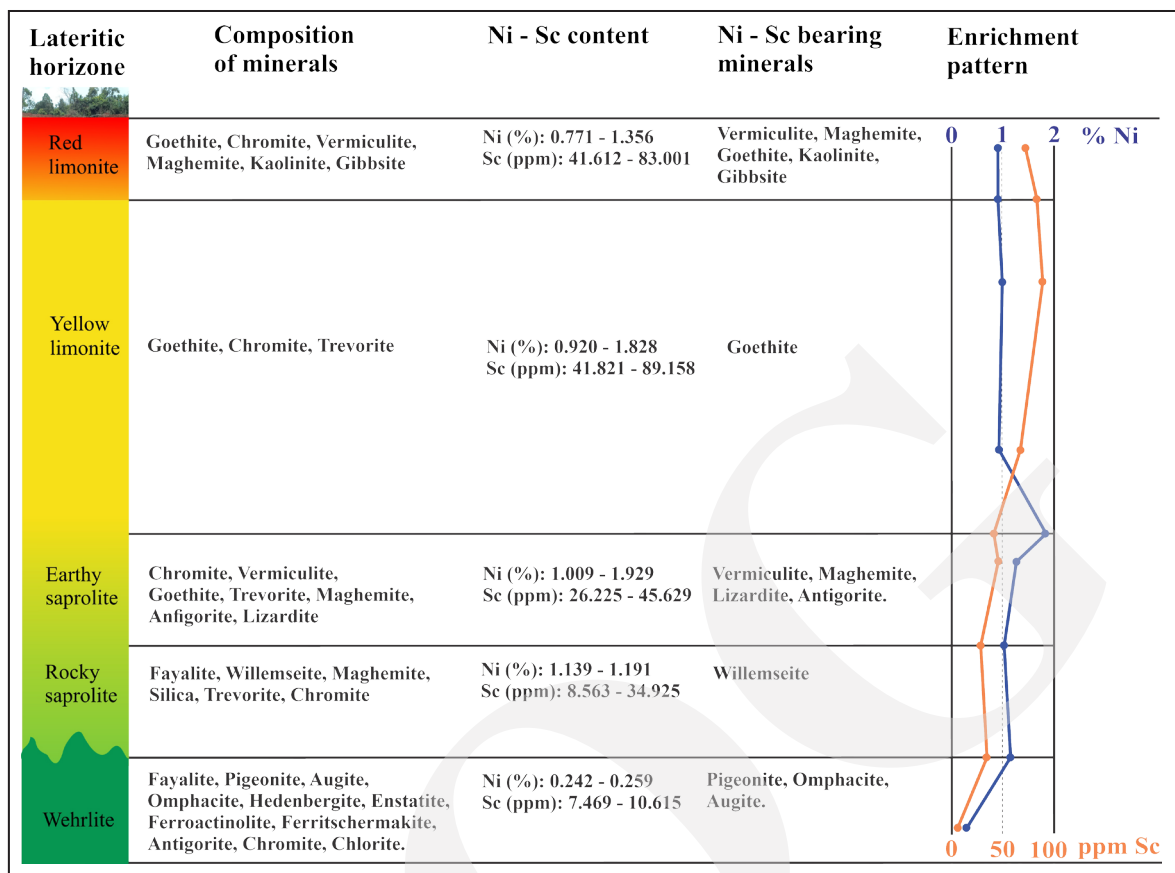
Lateritic horizone	Composition of minerals	Ni - Sc content	Ni - Sc bearing minerals	Enrichment pattern
Red limonite	Goethite, Chromite, Vermiculite, Maghemite, Kaolinite, Gibbsite	Ni (%): 0.771 - 1.356 Sc (ppm): 41.612 - 83.001	Vermiculite, Maghemite, Goethite, Kaolinite, Gibbsite	
Yellow limonite	Goethite, Chromite, Trevorite	Ni (%): 0.920 - 1.828 Sc (ppm): 41.821 - 89.158	Goethite	
Earthy saprolite	Chromite, Vermiculite, Goethite, Trevorite, Maghemite, Anfigorite, Lizardite	Ni (%): 1.009 - 1.929 Sc (ppm): 26.225 - 45.629	Vermiculite, Maghemite, Lizardite, Antigorite.	
Rocky saprolite	Fayalite, Willemseite, Maghemite, Silica, Trevorite, Chromite	Ni (%): 1.139 - 1.191 Sc (ppm): 8.563 - 34.925	Willemseite	
Wehrlite	Fayalite, Pigeonite, Augite, Omphacite, Hedenbergite, Enstatite, Ferroactinolite, Ferritschermakite, Antigorite, Chromite, Chlorite.	Ni (%): 0.242 - 0.259 Sc (ppm): 7.469 - 10.615	Pigeonite, Omphacite, Augite.	

Figure 18. Lateritic horizons and their mineral composition in relation to the bearing minerals and enrichment of Ni-Sc at the studied area.

CONCLUSION

This research examines the lateritization process of ultramafic rocks and the resultant enrichment of nickel and scandium in the Lameruru area. The study focuses on the mineralogical and geochemical transformations that occur from the parent rock (wehrlite) through the different laterite horizons: rocky saprolite, earthy saprolite, yellow limonite, and red limonite.

Intense chemical weathering during lateritization alters the primary silicate minerals (clinopyroxene, orthopyroxene, and olivine) in the wehrlite into secondary minerals. These include willemseite, vermiculite, lizardite, antigorite, maghemite, goethite, gibbsite, and kaolinite. Those secondary minerals play a crucial role in hosting Ni and Sc.

Ni enrichment is highest in the saprolitic horizon and decreases towards the red limonite. This

suggests an initial enrichment during weathering followed by possible remobilization and depletion in the upper horizons.

Sc enrichment, unlike Ni, shows a continuous increase throughout the profile, peaking in the red limonite. This contrasting behaviour indicates different geochemical controls on the two elements. The abundance of Sc-bearing goethite in the red limonite correlates strongly with the Sc enrichment.

Ni is found in almost all secondary minerals, while Sc is primarily associated with goethite, gibbsite, kaolinite, and maghemite, particularly in the red limonite. This suggests that Ni is structurally bound within the mineral lattices, whereas Sc is likely adsorbed onto mineral surfaces.

Further research in Lameruru area should investigate the specific geochemical mechanisms responsible for the contrasting behaviour of Ni and Sc, including the roles of pH, Eh, and the in-

fluence of organic matter. A deeper understanding of the adsorption processes governing Sc enrichment could inform strategies for optimizing Sc recovery. The findings of this study contribute to a better understanding of laterite formation and the enrichment of critical metals like Ni and Sc, which are essential for various industrial applications

References

Altinsel, Y., Topkaya, Y., Kaya, Ş., and Şentürk, B., 2018. Extraction of Scandium from Lateritic Nickel-Cobalt Ore Leach Solution by Ion Exchange: A Special Study and Literature Review on Previous Works. *The Minerals, Metals & Materials Series* p.1545. DOI: 10.1007/978-3-319-72284-9_201.

Anderson, C., 2018. Critical Metals Research from Primary and Secondary Sources at KIEM. *International Journal of the Society of Materials Engineering for Resources,* 23 (2), p.123. DOI: 10.5188/ijsmer.23.123.

Bai, Y., Su, B., Xiao, Y., Chen, C., Cui, M., Hen, Z., Qin, L., and Charlier, B., 2019. Diffusion-driven chromium isotope fractionation in ultramafic cumulate minerals: Elemental and isotopic evidence from the Stillwater Complex. *Geochimica et Cosmochimica Acta,* 263, p.167. DOI: 10.1016/j.gca.2019.07.052.

Butt, C.R.M. and Wang, B., 2013. *Nickel Laterite Ore Deposits: Weathered Serpentinites. Elements,* 9 (2), p.123. DOI: 10.2113/gselements.9.2.123.

Chassé, M., Griffin, W.L., O'Reilly, S.Y., and Calas, G., 2016. Scandium speciation in a world-class lateritic deposit. *Geochemical Perspectives Letters,* p.105. DOI: 10.7185/geochemlet.1711.

Cui, T., 2018. Distribution Characteristics of Rare, Rare Earth and Scattered Element in Southwestern Guizhou. *IOP Conference Series Earth and Environmental Science,* 170, 22084. DOI: 10.1088/1755-1315/170/2/022084.

Cui, T. and Nie, A., 2018. Geological Features of Scandium Deposits in Southwestern Guizhou Province. *IOP Conference Series Earth and Environmental Science,* 170, 22183. DOI: 10.1088/1755-1315/170/2/022183.

Czerwiński, F., 2022. Critical Minerals for Zero-Emission Transportation [Review of Critical Minerals for Zero-Emission Transportation]. *Materials,* 15 (16), 5539. DOI: 10.3390/ma15165539.

Dilshara, R.M.P., Abeysinghe, B., Premasiri, R., Dushyantha, N., Ratnayake, N. P., Senarath, S., Ratnayake, A.S., and Batapola, N., 2023. The role of nickel (Ni) as a critical metal in clean energy transition: applications, global distribution and occurrences, production-demand and phytomining. *Journal of Asian Earth Sciences,* 259, 105912.

Emsley, J., 2014. *Unsporting scandium. Nature Chemistry,* 6 (11), 1025. DOI: 10.1038/nchem.2090.

Ent, A. van der, Baker, A. J. M., Balgooy, M.M.J. van, and Tjoa, A.M., 2013. Ultramafic nickel laterites in Indonesia (Sulawesi, Halmahera): Mining, nickel hyperaccumulators and opportunities for phytomining. *Journal of Geochemical Exploration,* 128, p.72-79. DOI: 10.1016/j.gexplo.2013.01.009.

Farrokhpay, S., Filippov, L.O., and Fornasiero, D., 2019. Pre-concentration of nickel in laterite ores using physical separation methods. *Minerals Engineering,* 141, 105892. DOI: 10.1016/j.mineng.2019.105892.

Fu, W., Yang, J., Yang, M., Pang, B., Liu, X., Hu-Jie, N., and Huang, X., 2014. Mineralogical and geochemical characteristics of a serpentinite-derived laterite profile from East Sulawesi, Indonesia: Implications for the lateritization process and Ni supergene enrichment in the tropical rainforest. *Journal of Asian Earth Sciences,* 93, p.74-88. DOI: 10.1016/j.jseaes.2014.06.030.

Garnier, J., Quantin, C., Guimarães, E.M., Garg, V.K., Martins, E.S., and Becquer, T., 2009. Understanding the genesis of ultramafic soils and catena dynamics in Niquelândia, Brazil. *Geoderma,* 151 (3-4), p.204-214. DOI: 10.1016/j.geoderma.2009.04.020.

Hall, R. and Wilson, M.E.J., 2000. Neogene sutures in eastern Indonesia. *Journal of Asian Earth Sciences,* 18, p.781-808. DOI: 10.1016/S1367-9120(00)00040-7.

Hughes, H.S.R., Andersen, J.C.Ø., and O'Driscoll, B., 2020. Mineralization in Layered Mafic-Ultramafic Intrusions. *Elsevier eBooks,* 823pp. DOI: 10.1016/b978-0-08-102908-4.00037-0.

Kadarusman, A., Miyashita, S., Maruyama, S., Parkinson, C.D., and Ishikawa, A., 2004. Petrology, geochemistry and paleogeographic reconstruction of the East Sulawesi Ophiolite, Indonesia. *Tectonophysics,* 392 (1), p.55-83. DOI: 10.1016/j.tecto.2004.04.008.

Koch, J.C., Connolly, C.T., Baughman, C., Repasch, M., Best, H., and Hunt, A., 2022. Geology, Minerals, Energy, and Geophysics Science Center. https://www.usgs.gov/centers/gmeg.

Konopka, G., Szamałek, K., and Zglinicki, K., 2022. Ni-Co Bearing Laterites from Halmahera Island (Indonesia). *Applied Sciences,* 12 (15), 7586. DOI: 10.3390/app12157586.

Li, G., Shi, T., Rao, M., Jiang, T., and Zhang, Y., 2012. Beneficiation of nickeliferous laterite by reduction roasting in the presence of sodium sulfate. *Minerals Engineering,* 32, p.19-26. DOI: 10.1016/j.mineng.2012.03.012.

Maulana, A., Christy, A.G., and Ellis, D.J., 2014. Petrology, geochemistry and tectonic significance of serpentinized ultramafic rocks from the South Arm of Sulawesi, Indonesia. *Geochemistry,* 75 (1), p.73-87. DOI: 10.1016/j.chemer.2014.09.003.

Maulana, A., Sufriadin, S., Sanematsu, K., and Sakakibara, M., 2019. Study on Sc-bearing Lateritic Ni deposits in Ultramafic Rock from Sulawesi: A New Paradigm in Indonesia Metal Mining Industry. *IOP Conference Series Materials Science and Engineering,* 676 (1), 12032. DOI: 10.1088/1757-899x/676/1/012032.

Maurizot, P., Sevin, B., Iseppi, M., and Giband, T., 2019. Nickel-Bearing Laterite Deposits in Accretionary Context and the Case of New Caledonia: From the Large-Scale Structure of Earth to Our Everyday Appliances. *GSA Today,* 29 (5), p.4-10. DOI: 10.1130/gsatg364a.1.

Mawaleda, M., Husain, J.R., Forster, M., Suparka, E., Abdullah, C.I., Basuki, N.I., and Hutabarat, J., 2018. Miocene tectonic of the Southeast Arm of Sulawesi, Indonesia: Based on petrology data, geochemistry, and 40Ar/39Ar geochronology of metamorphic rocks from Rumbia Complex. *IOP Conference Series: Earth and Environmental Science,* 212, 12043. DOI: 10.1088/1755-1315/212/1/012043.

Muñoz, M., Ulrich, M., Cathelineau, M., and Mathon, O., 2018. Weathering processes and crystal chemistry of Ni-bearing minerals in saprock horizons of New Caledonia ophiolite. *Journal of Geochemical Exploration,* 198, p.82-99. DOI: 10.1016/j.explo.2018.12.007.

Orberger, B. and Ent, A. van der., 2019. Nickel laterites as sources of nickel, cobalt and

scandium: Increasing resource efficiency through new geochemical and biological insights. *Journal of Geochemical Exploration,* 204, p.297-299. DOI: 10.1016/j.gexplo.2019.06.004.

Qin, H., Yang, S., Tanaka, M., Sanematsu, K., Arcilla, C. A., and Takahashi, Y., 2020. Chemical speciation of scandium and yttrium in laterites: New insights into the control of their partitioning behaviors. *Chemical Geology,* 552, 119771. DOI: 10.1016/j.chemgeo.2020.119771.

Quast, K., Addai-Mensah, J., and Skinner, W., 2017. Preconcentration strategies in the processing of nickel laterite ores Part 5: Effect of mineralogy. *Minerals Engineering,* 110, p.31-39. DOI: 10.1016/j.mineng.2017.03.012.

Røyset, J. and Ryum, N., 2005. Scandium in aluminium alloys. *International Material Reviews*, 50 (1), p.19-44. DOI: 10.1179/174328005X14311.

Rusmana, E., Sukarna, D., Haryono, E., and Simandjuntak, T.O., 1993. *Geologi Lembar Lasusua-Kendari, Sulawesi, skala 1:250.000.* Pusat Penelitian dan Pengembangan Geologi. Direktorat Jenderal Geologi dan Sumberdaya Mineral.

Sanematsu, K., Maulana, A., Yokoyama, T.D., and Kon, Y., 2017. Scandium-Bearing Minerals in Lateritic Nickel Ores of the Soroako Deposit in Indonesia. https://www.segweb.org/SEG/Events/Conference-Archive/2017/Conference-Proceedings/ files/pdf/Poster-Presentations/Abstracts/P158-Sanematsu.pdf.

Sharma, S., 2021. Critical Minerals: Current Challenges and Future Strategies. *International Journal of Environmental Sciences and Natural Resources,* 27 (3), 556215. DOI: 10.19080/ijesnr.2021.27.556215.

Tamehe, L.S., Zhao, Y., Xu, W., and Gao, J., 2024. Ni (Co) laterite deposits of southeast asia: A review and perspective. *Minerals,* 14 (2), 134. DOI: 10.3390/min14020134.

Tauler, E., Llovet, X., Villanova-de-Benavent, C., Chang-Rodríguez, A., Núñez-Cambra, K., Khazaradze, G., and Proenza, J.A., 2023. Geochemistry and mineralogy of the clay-type ni-laterite deposit of san felipe (camagüey, cuba). *Minerals,* 13 (10), 1281. DOI: 10.3390/min13101281.

Teitler, Y., Cathelineau, M., Ulrich, M., Ambrosi, J.P., Muñoz, M., and Sevin, B., 2018. Petrology and geochemistry of scandium in New Caledonian Ni-Co laterites. *Journal of Geochemical Exploration,* 196, 131. DOI: 10.1016/j.explo.2018.10.009.

Toropova, L.S., Eskin, D.G., Kharakterova, M.L., and Dobatkina, T.V., 2017. *Advanced aluminum alloys containing scandium structure and properties.* Taylor & Francis Group. DOI: 10.4324/9781315097541.

Tupaz, C.A.J., Watanabe, Y., Sanematsu, K., and Echigo, T., 2020. Mineralogy and geochemistry of the Berong Ni-Co laterite deposit, Palawan, Philippines. *Ore Geology Reviews,* 125, 103686. DOI: 10.1016/j.oregeorev.2020.103686.

Ulrich, M., Cathelineau, □Michel, Muñoz, M., Boiron, M., Teitler, Y., and Karpoff, A. M., 2018. The relative distribution of critical (Sc, REE) and transition metals (Ni, Co, Cr, Mn, V) in some Ni-laterite deposits of New Caledonia. *Journal of Geochemical Exploration,* 197, p.93-113. DOI: 10.1016/j.gexplo.2018.11.017.

Wang, W., Pranolo, Y., and Cheng, C. Y., 2011. Metallurgical processes for scandium recovery from various resources: A review. *Hydrometallurgy,* 108 (1), p.100-108. DOI: 10.1016/j.hydromet.2011.03.001.

Wang, Z., Li, Y., Liu, Z.-R. R., and Zhou, M., 2020. Scandium: Ore deposits, the pivotal role of magmatic enrichment and future exploration. *Ore Geology Reviews*, 128, 103906. DOI: 10.1016/j.oregeorev.2020.103906.

Williams-Jones, A.E. and Vasyukova, O.V., 2018. The Economic Geology of Scandium, the Runt of the Rare Earth Element Litter. *Economic Geology,* 113 (4), p.973-988. DOI: 10.5382/econgeo.2018.4579.

Wilson, M.J., 2004. Weathering of the primary rock-forming minerals: processes, products and rates. *Clay Minerals,* 39 (3), p.233-236. DOI: 10.1180/0009855043930133.

Xiao, J., Xiong, W., Zou, K., Chen, T., Li, H., and Wang, Z., 2021. Extraction of nickel from Magnesia–Nickel silicate ore. *Journal of Sustainable Metallurgy,* 7, p.642-652. DOI: 10.1007/s40831-021-00364-0.